TISSUE ENGINEERING
Volume 10, Number 5/6, 2004

Tissue Engineering Using Magnetite Nanoparticles and Magnetic Force: Heterotypic Layers of Cocultured Hepatocytes and Endothelial Cells

AKIRA ITO, Ph.D.,[1] YOHEI TAKIZAWA, M.Eng.,[1] HIROYUKI HONDA, Ph.D.,[1] KEN-ICHIRO HATA, D.D.S., Ph.D.,[2] HIDEAKI KAGAMI, D.D.S., Ph.D.,[3] MINORU UEDA, D.D.S., Ph.D.,[4] and TAKESHI KOBAYASHI, Ph.D.[1]

ABSTRACT

Novel technologies to establish three-dimensional, *in vivo*-like tissue consisting of various types of cells are required for tissue engineering. We applied magnetic force to construct a heterotypic, layered coculture system of rat hepatocytes and human aortic endothelial cells (HAECs) that was not limited by cell type. Magnetite cationic liposomes carrying a positive surface charge to improve adsorption accumulated in HAECs at a concentration of 38 pg of magnetite per cell. Magnetically labeled HAECs specifically accumulated onto hepatocyte monolayers at sites where a magnet (4000 G) was positioned, and then adhered to form a heterotypic, layered construct with tight and close contact. This cocultured construct significantly ($p < 0.05$) enhanced albumin secretion by hepatocytes compared with that in homotypic cultures of hepatocytes or heterotypic cocultures of hepatocytes and HAECs without magnets. These results suggest that this novel use of magnetite nanoparticles and magnetic force, which we refer to as "magnetic force-based tissue engineering" (Mag-TE), offers a major advancement in tissue engineering.

INTRODUCTION

TISSUE ENGINEERING holds much promise as a means of resolving various issues surrounding organ transplantation. Tissues and organs *in vivo* are often composed of several types of cell layers. Cell–cell interactions among these are important to maintain the normal physiology of organ systems such as the vasculature (smooth muscle and endothelial cells),[1] skeletal muscle (myocytes and peripheral nerves),[2] and liver (hepatocytes and sinusoidal endothelial cells).[3] However, cell–cell interactions are difficult to manipulate in coculture systems with two or more cell types even in two-dimensional (2D) cultures. Moreover, the assembly of three-dimensional (3D) tissues containing various cell types remains a challenge.

Heterotypic interactions play a fundamental role in liver function. Because the liver is formed from the endodermal foregut and mesenchymal vascular structures, it might be functionally mediated by heterotypic interactions.[4,5] Liver-specific functions in isolated hepatocytes that require nonparenchymal cells disappear in homotypic cultures.[6] Various 2D coculture systems of hepato-

[1]Department of Biotechnology, School of Engineering, Nagoya University, Nagoya, Japan.
[2]Genetic and Regenerative Medical Center, School of Medicine, Nagoya University, Nagoya, Japan.
[3]Department of Tissue Engineering, School of Medicine, Nagoya University, Nagoya, Japan.
[4]Department of Oral and Maxillofacial Surgery, School of Medicine, Nagoya University, Nagoya, Japan.

cytes and nonparenchymal cells have been investigated, including those using microfabrication[7] and 2D patterning.[8] However, novel technologies are required to reconstruct the liver to function as it does *in vivo*. This would require a 3D construct containing various types of cells that could thrive beyond the cell type limitations of coculture. The present study uses magnetic force to precisely place magnetically labeled cells onto target cells and to promote heterotypic cell–cell adhesion to form a 3D construct.

Many biological and medical applications have used magnetite particles ranging in size from nanometers to micrometers. Because magnetite particles are attracted to a high magnetic flux density, fine magnetite particles can label biomolecules or living cells so that cells of interest can be specifically separated.[9–12] We developed magnetite cationic liposomes (MCLs) containing magnetite nanoparticles that electrostatically interact with the cell membrane.[13] The affinity of MCLs for tumor cells is 10-fold higher than that of neutral liposomes containing magnetite nanoparticles.[13] Therefore, MCLs are suitable for magnetically labeling live cells and have functioned as carriers to introduce DNA into cells,[14] and as heat-generating mediators for hyperthermia.[15–18] Here, we magnetically labeled human aortic endothelial cells (HAECs) using MCLs. We then investigated whether the labeled HAECs could be placed onto a rat hepatocyte layer, using magnetic force, and whether magnetic force promotes the adhesion of heterotypic cells.

MATERIALS AND METHODS

Cells and culture

Human aortic endothelial cells (HAECs) at the third passage obtained from Cambrex Bio Science Walkersville (Walkersville, MD) were cultured at 37°C in a humidified atmosphere of 5% CO_2 and 95% air in HAEC growth medium (EGM-2; Cambrex Bio Science Walkersville).

Hepatocytes were isolated from 7- to 9-week-old Sprague-Dawley rats, using conventional *in situ* collagenase perfusion and low-speed centrifugation with slight modification.[18,19] The total liver cell suspension was separated by centrifugation at $50 \times g$ for 1 min and sedimented cells were further purified by repeated centrifugation at $50 \times g$ for 1 min to obtain parenchymal hepatocytes. Isolated hepatocytes were seeded on type I collagen-coated 24-well plates (Asahi Techno Glass, Chiba, Japan) at a density of 6×10^4 cells /cm^2, and cultured in Williams' medium E (GIBCO-BRL, Grand Island, NY) supplemented with 0.1 μM $CuSO_4 \cdot 5H_2O$, 25 nM Na_2SeO_3, 1.0 μM $ZnSO_4 \cdot 7H_2O$, 0.1 μM insulin (Sigma, St. Louis, MO), 1.0 μM dexamethasone (Wako, Osaka, Japan), epidermal growth factor (20 μg/liter; Sigma), gentamicin sulfate (48 mg/liter; Wako), chloramphenicol (100 mg/liter; Wako), and 5% fetal bovine serum.

Preparation of magnetite cationic liposomes

The magnetite (Fe_3O_4; average particle size, 10 nm) used as the core of the MCLs was donated by Toda Kogyo (Hiroshima, Japan). We prepared MCLs using colloidal magnetite and a lipid mixture of *N*-(α-trimethylammonioacetyl)-didodecyl-D-glutamate chloride, dilauroylphosphatidylcholine, and dioleoylphosphatidyl-ethanolamine in a 1:2:2 molar ratio as described.[13]

MCL uptake by HAECs

We examined the uptake of MCLs by HAECs as described.[13] Briefly, HAECs (5×10^4 cells) were seeded into 6-well cell culture plates (Asahi Techno Glass) containing 2 mL of EGM-2. After 24 h, the medium was replaced with EGM-2 containing MCLs (net magnetite concentration, 100 pg/cell) and the cells were incubated once more. The cells were sampled periodically to measure iron concentration and cell number using potassium thiocyanate[20] and trypan blue dye exclusion, respectively.

Layered coculture of hepatocytes and HAECs, using magnetic force

Primary rat hepatocytes were cultured for 2 days and then cocultured with HAECs magnetically labeled with MCLs. Eight hours after adding MCLs, 1.2×10^5 HAECs were seeded onto the monolayer hepatocyte surface. A cubical or cylindrical neodymium magnet (diameter, 3 or 22 mm; height, 3 or 10 mm; magnetic induction, 4000 G, respectively) was then placed under the 24-well plates to provide magnetic force vertical to the plate, and the plate was shaken in a figure-eight pattern (Taitec, Tokyo, Japan). The magnetic flux of the magnets was measured with a hand-held gauss meter (F.W. Bell, Orlando, FL). One day after the start of coculture, the cells were cultured in a mixture of HAEC (EGM-2) and hepatocyte (Williams' medium E) medium in a 1:1 ratio. The magnets were removed on day 2 after starting the coculture.

Histology

On day 2 after the start of coculture, the cells were washed with phosphate-buffered saline (PBS) twice, fixed in 10% formalin, and embedded in paraffin. Thin (4 μm) slices from paraffin-embedded specimens were deparaffinized in xylene and rehydrated in an ethanol se-

ries. The sections were incubated with 10% skim milk at 37°C for 10 min to block background staining, followed by incubations at 37°C for 60 min each with sheep IgG fraction to rat albumin (ICN Biomedicals, Aurora, OH) and biotinylated goat anti-sheep IgG (Dako Cytomation, Kyoto, Japan). Thereafter, the slices were incubated at 37°C for 30 min with peroxidase-conjugated streptavidin (Dako Cytomation). Each step was followed by a PBS wash. Peroxidase activity was visualized after soaking the slices at room temperature for 10 min in 0.02% diaminobenzidine tetrahydrochloride containing 0.005% hydrogen peroxide. Slides were also double stained with anti-albumin antibodies and with Berlin blue,[21] which colored the peroxidase activity of albumin brown and magnetite in MCLs blue. All sections, except for those that were double stained, were also stained with hematoxylin and eosin. Primary antibodies were replaced in negative control sections with either an irrelevant monoclonal antibody or PBS.

Albumin assay

The albumin concentration in the medium was determined by a sandwich solid-phase enzyme-linked immunosorbent assay (ELISA),[19] using anti-rat albumin and peroxidase-conjugated anti-rat albumin antibodies (ICN Biomedicals) and purified rat albumin (Sigma) as the standard.

Statistical analysis

The Mann–Whitney rank sum test evaluated the statistical significance of differences. Statistically significant differences were established at a p value below 0.05.

RESULTS

Magnetite nanoparticle uptake by HAECs and the effect on proliferation

We examined uptake of MCLs containing 100 pg of magnetite per cell in EGM-2. The uptake of magnetite nanoparticles began rapidly, reaching a maximum (38 pg/cell) 8 h after addition (Fig. 1A). Subsequently, the amount of magnetite per cell decreased because of dilution resulting from cell growth. The color of HAECs containing MCLs became black-brown, which is the color of magnetite. We compared the growth of HAECs in medium with and without MCLs to determine the toxicity of MCLs for HAECs (Fig. 1B). The inclusion of MCLs (100 pg/cell) in the medium did not inhibit the growth of HAECs. Therefore, HAECs were mixed with MCLs containing magnetite at 100 pg/cell and were magnetically labeled for 8 h in the following studies.

Layered coculture of HAECs and hepatocytes, using magnetite nanoparticles and magnetic force

We investigated whether magnetic force can regulate the positioning of magnetically labeled cells, using 3-mm magnets (surface area of 9 mm^2 was smaller than the 200-mm^2 culture area of 24-well culture plates). Figure 2A shows the magnetic flux density of the 3-mm magnet.

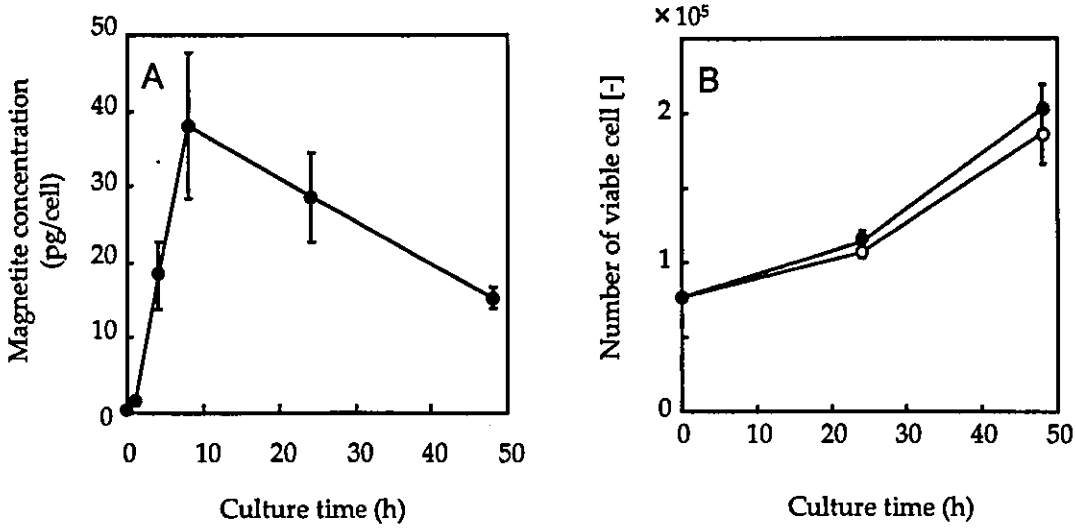

FIG. 1. MCL uptake and HAEC proliferation. Magnetite nanoparticle uptake after adding MCLs (100 pg/cell), measured with potassium thiocyanate. (**B**) Toxicity of MCLs against HAECs, determined by measuring cell growth after adding MCLs. Open circles, no MCLs; solid circles, with MCLs (100 pg/cell). Data points represent means and SD of triplicates.

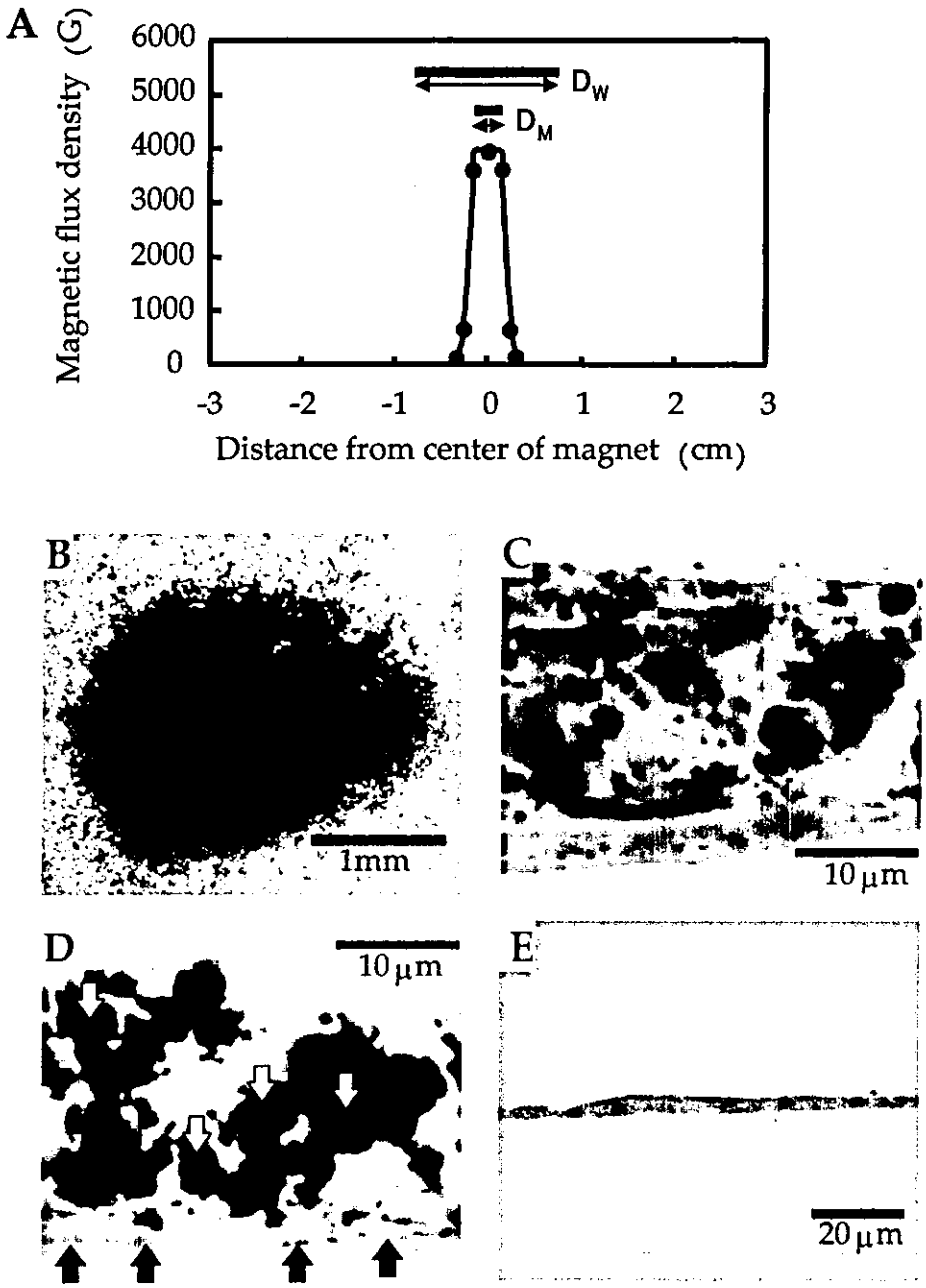

FIG. 2. Construction of 3D coculture of HAECs and hepatocytes, using 3–mm magnets. HAECs were incubated in medium containing MCLs for 8 h and seeded onto rat hepatocyte monolayers; the magnet was then positioned. (**A**) Magnetic flux density around the neodymium magnet. D_M, diameter of magnet (3 mm); D_w, diameter of the cell culture well (15.5 mm). (**B**) State of HAECs accumulated by magnetic force at 2 days after coculture. (**C**) HAECs labeled with MCLs appear black-brown. (**C** and **E**) Bright-field photographs of hematoxylin- and eosin-stained sections of cocultured hepatocytes and HAECs inside (**C**) or outside (**E**) the magnet position. (**D**) Immunohistochemical stain for albumin (brown, indicated by solid arrows) double-stained with Berlin blue (blue, indicated by open arrows).

Magnetic density (4000 G) was detected only at the surface of the magnet. Figure 2B shows phase-contrast microscopy of HAECs trapped by the magnetic force. Black-brown HAECs accumulated on the hepatocyte layer at the center of dishes where magnets were placed. These HAECs remained attached to the hepatocyte layer when the magnet was removed on day 2 after coculture, and even after vigorous agitation of the culture plates or pipetting. To confirm that HAEC layers were firmly attached to the hepatocyte monolayer, we examined cross-sections of the layers. We found a construct (Fig. 2C) consisting of a hepatocyte monolayer that expressed al-

bumin under thick Berlin blue-positive HAEC layers (Fig. 2D). On the other hand, few HAECs adhered in areas where magnets were not located (Fig. 2E).

Liver function in layered cocultures of HAECs and hepatocytes, using magnetite nanoparticles and magnetic force

We seeded 1.2×10^5 HAECs (the number of cells required to reach confluence in 24-well cell culture plates) onto hepatocyte monolayers and placed a 22-mm magnet with a surface area of 380 mm^2, which was larger than the culture area of the plate (200 mm^2), to form double cell layers throughout the wells. Figure 3A shows the magnetic flux density of the 22-mm magnet. The magnetic density (4000 G) detected at the surface of the magnet was essentially even throughout the culture areas of the 24-well plates. HAECs labeled (Fig. 3B and D) or not (data not shown) with MCLs did not attach to hepatocytes in the absence of a magnet. On the other hand, in the presence of the 22-mm magnet, HAECs evenly attached to the hepatocyte layer throughout the wells (Fig. 3C). The hepatocyte layer expressed albumin under the HAEC monolayer that stained positively with Berlin blue, indicating the presence of MCLs (Fig. 3E).

We measured hepatic albumin expression to determine cellular function in the layered coculture system using 22-mm magnets (Fig. 4). Albumin secretion in homotypic hepatocyte culture was undetectable beyond 5 days of culture. Hepatic albumin secretion was slightly enhanced in cocultures of HAECs labeled with and without MCLs, even when the magnet was not positioned. On the other

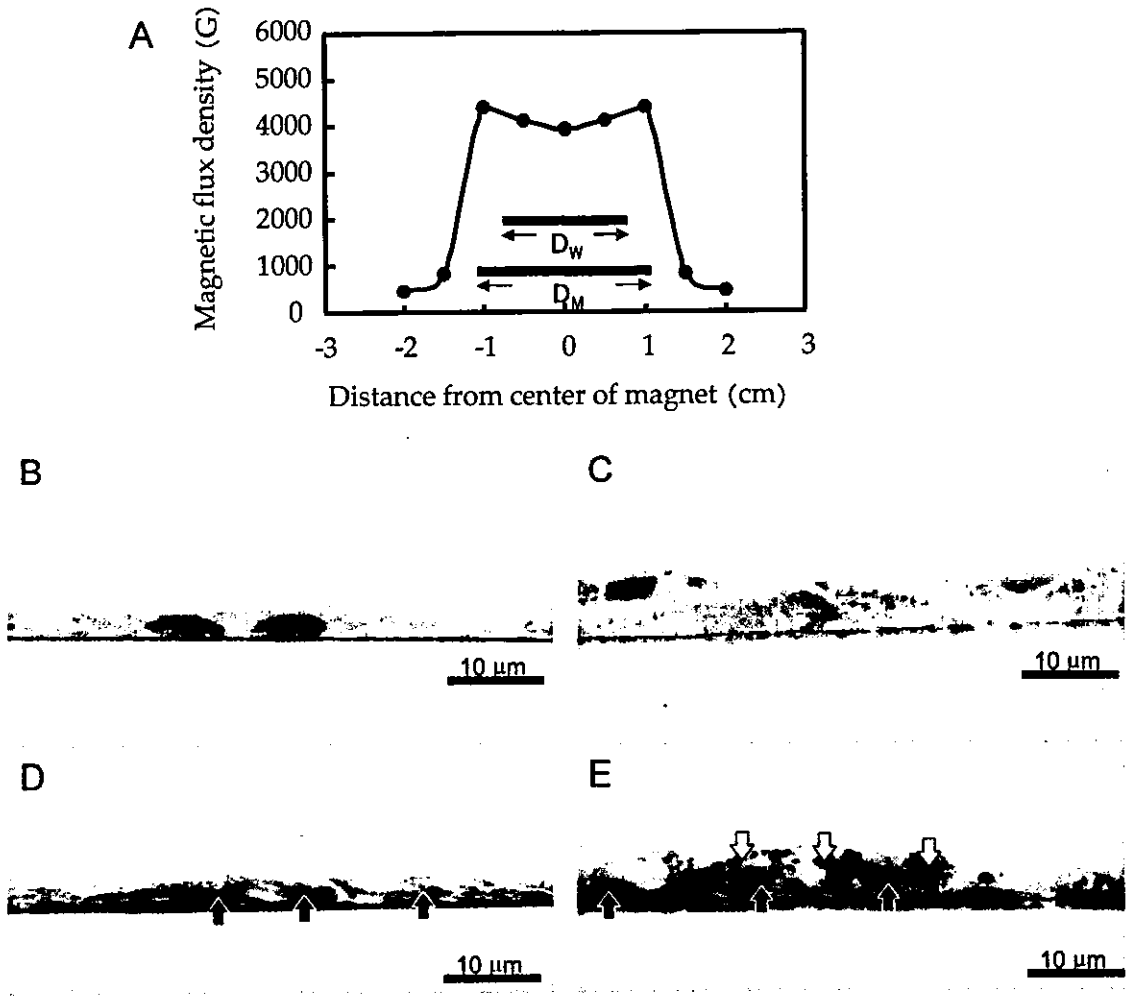

FIG. 3. Construction of 3D HAEC and hepatocyte cocultures, using 22–mm magnets. HAECs were incubated in medium containing MCLs for 8 h and seeded onto rat hepatocyte monolayers; the magnet was then positioned. (**A**) Magnetic flux density around the neodymium magnet. D_m, diameter of magnet (22 mm); D_w, diameter of the cell culture well (15.5 mm). (**B** and **C**) Bright-field photographs of hematoxylin- and eosin-stained sections of cocultured hepatocytes and HAECs without (**B**) or with (**C**) the magnet. (**D** and **E**) Immunohistochemical results for albumin (brown, indicated by solid arrows) double-stained with Berlin blue (blue, indicated by open arrows) in the coculture without (**D**) or with (**E**) the magnet.

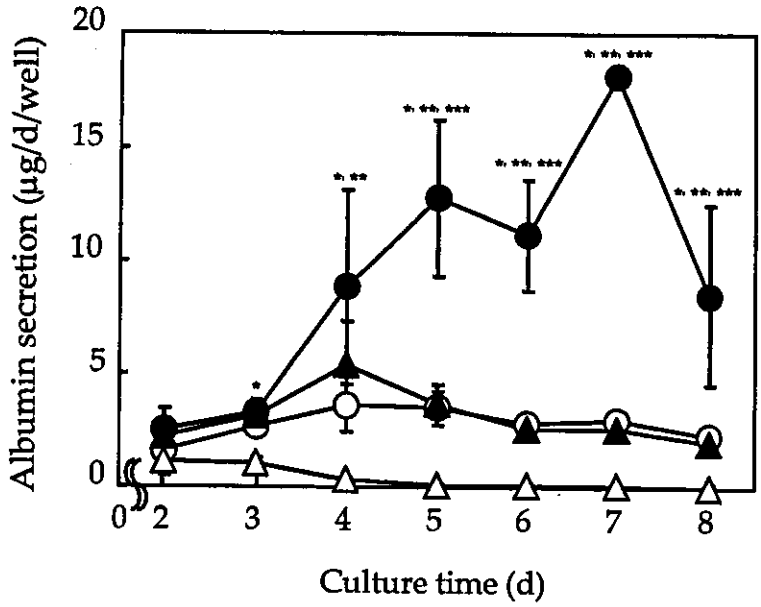

FIG. 4. Albumin secretion by rat hepatocytes under different culture conditions. Hepatocytes were initially cultured for 2 days to form monolayers. Open triangles, hepatocytes incubated alone as homotypic cultures; solid triangles, HAECs seeded onto hepatocytes; open circles, HAECs labeled with MCLs and seeded onto hepatocytes without magnets; solid circles, HAECs labeled with MCLs, seeded onto hepatocytes with magnets, and then cultured for 8 days. Albumin secretion from hepatocytes was significantly enhanced when HAECs labeled with MCLs were seeded onto hepatocytes with magnets (solid circles) compared with homotypic cultures of hepatocytes (open triangles, $*p < 0.05$) and heterotypic cocultures of HAECs labeled without (open circles, $**p < 0.05$) or with (solid triangles, $***p < 0.05$) MCLs in the absence of magnets. The experiment was performed three times, and each point represents the mean ± SD.

hand, layered cocultures in the presence of a magnetic force maintained a high level of albumin secretion throughout the study.

DISCUSSION

Two major difficulties obstruct fabrication of an *in vivo*-like 3D construct for 3D tissue engineering including heterotypic cells. One is nonadherence to heterotypic cells caused by the cell type limitation of coculture. Okano and colleagues developed double-layered cocultures using a thermoresponsive surface of grafted poly(*N*-isopropylacrylamide) (PIPAAm) to overcome this difficulty, and termed the method "cell sheet engineering."[22–24] Harimoto *et al.*[25] reported that whereas trypsinized single endothelial cells do not attach to hepatocytes, endothelial cell sheets fabricated by cell sheet engineering could attach to hepatocyte monolayers. However, the assembly of heterotypic cells into complex tissues such as ductlike constructs also presents a challenging technological barrier even for cell sheet engineering. Another difficulty is to spatially control the positioning of target cells. Mironov *et al.*[26] developed a computer-aided jet-based cell printer that could place cells at specific sites on thermoresponsive gels and termed this "organ printing." This technology seemed to overcome the difficulties with spatial control. However, printed cells can form only monolayers that must be stratified layer by layer to assemble 3D organs. Here, we developed a new method using magnetite nanoparticles and magnetic force, which we refer to as "magnetic force-based 3D tissue engineering," to overcome these difficulties.

Figure 3B and D shows that HAECs did not attach onto rat hepatocytes, which agrees with the results of Harimoto *et al.*[25] On the other hand, HAECs magnetically labeled with MCLs attached to hepatocytes in the presence of a magnetic force (Fig. 3C and E). Kushida *et al.*[27] recovered monolayer cell sheets from a surface grafted with PIPAAm and deposited extracellular matrices (ECMs); the remaining ECMs enhanced cell–cell attachment because digestive enzymes such as trypsin were unnecessary. Because we used trypsin in the present study, the ECMs of HAECs magnetically labeled with MCLs did not attach to hepatocytes without a magnet because their ECMs may be digested. As an alternative way to enhance layered cell–cell interactions, we applied a physical approach using magnetic attraction. On day 2 after coculture, HAECs remained attached to the hepatocyte layer and did not detach after either vigorously agitating the culture plates or pipetting (Figs. 2 and 3). We suppose that the cell–cell adhesion was caused by the close placement of heterotypic cells for by the magnetic force, af-

ter which the ECMs may form tight cell–cell interactions. The mechanisms of the cell–cell adhesion initiated by a physical approach using magnets and the subsequent deposition of ECMs remain to be further examined.

The magnetic force allowed the spatial control of magnetically labeled cells. Figure 2 shows that the culture area of the HAECs magnetically labeled with MCLs was restricted by the magnetic force. When an excess of cells (1.2×10^5) compared with the size of magnet (3 mm; area, 9 mm^2) was applied, "multilayered" HAECs developed on hepatocyte monolayers where the magnet was located, and cells that overflowed from the multilayer site did not attach to hepatocytes. These results suggested that the magnetic force can regulate the culture space, and that multilayered constructs can be generated simply by calculating the number of cells against the culture space. However, some HAECs did not attach to the magnetically regulated culture area in the present study. This may be due to the relationship between the intensity of the applied magnetic force and the concentration of magnetite nanoparticles incorporated into the cells. Further examination is required because this relationship may differ among cell types.

Coculture systems with nonparenchymal cells maintain hepatocyte functions for long periods.[28–30] To examine the feasibility of the layered coculture system using magnetic force, we used the liver model of hepatocytes and endothelial cells. We seeded 1.2×10^5 HAECs, which corresponded to the number at confluence in 24-well cell culture plates, onto hepatocyte monolayers and positioned a 22-mm magnet that could apply 4000 G uniformly throughout the plates (Fig. 3A). This caused an almost uniform upper layer of HAECs (Fig. 3C and E). Albumin secretion by hepatocytes was enhanced in this double-layered coculture system (Fig. 4). The precise mechanisms that regulate increases in liver-specific function in hepatocyte cocultures have not been elucidated. Bhandari *et al.*[31] reported that 3T3 fibroblast cells persist in cocultures with hepatocytes, but 3T3 cell conditioned medium did not substitute for viable cocultured 3T3 cells in preserving hepatocyte function, suggesting that cell–cell interaction is essential for modulating hepatocyte functions. Potential mediators of cell–cell interactions include soluble factors such as cytokines[32] and insoluble cell-associated factors such as ECMs.[33] We surmise that the tight and close interaction of overlaying HAECs and monolayer hepatocytes using magnetic force caused ECMs and cytokines to be deposited between the layers, thus powerfully enhancing liver function (Fig. 4). In contrast, cellular interaction was weak in cocultures without the magnetic force and HAECs hardly attached to hepatocytes (Fig. 3B and D).

The toxicity of MCLs is important for clinical applications. We have used MCLs as a source of heat to generate hyperthermia, and examined their toxicity against cancer cells.[13] The MCLs were nontoxic against cell proliferation when the magnetite concentration was below 100 pg/cell. The present study examined toxicity against HAEC proliferation at a magnetite concentration of 100 pg/cell (Fig. 1B). At this concentration, 38% of the magnetite nanoparticles were incorporated by 8 h after MCL addition and these were diluted by HAEC proliferation (Fig. 1A). These results suggested that a magnetite concentration of 100 pg/cell is not toxic against HAEC proliferation.

In conclusion, we developed a novel methodology with which to construct 3D *in vivo*-like tissues, using magnetite nanoparticles and a magnetic force, which we call magnetic force-based tissue engineering (Mag-TE). This methodology, which allows the spatial control of target cells and the adherence of heterotypic cells using magnetic force, should be applied in the tissue engineering of complex 3D tissues.

ACKNOWLEDGMENTS

The authors thank Toda Kogyo for supplying the magnetite. This study was supported in part by the 21st Century COE Program, Nature-Guided Materials Processing, and by a Grant-in-Aid for Scientific Research (15760587) of the Ministry of Education, Science, Sports, and Culture of Japan.

REFERENCES

1. Fillinger, M.F., O'Connor, S.E., Wagner, R.J., and Cronenwett, J.L. The effect of endothelial cell coculture on smooth muscle cell proliferation. J. Vasc. Surg. **17,** 1058, 1993.
2. Coërs, C., and Woolf, A.L. The Innervation of Muscle. Springfield, IL: Charles C Thomas, 1959.
3. Guguen-Guillouzo, C., Clement, B., Baffet, G., Beaumont, C., Morel-Chany, E., Glaise, D., and Guillouzo, A. Maintenance and reversibility of active albumin secretion by adult rat hepatocytes co-cultured with another liver epithelial cell type. Exp. Cell Res. **143,** 47, 1983.
4. Houssaint, E. Differentiation of the mouse hepatic primordium. I. An analysis of tissue interactions in hepatocyte differentiation. Cell Differ. **9,** 269, 1980.
5. Douarin, N.M. An experimental analysis of liver development. Med. Biol. **53,** 427, 1975.
6. Bhatia, S.N., Balis, U.J., Yarmush, M.L., and Toner, M. Effect of cell–cell interactions in preservation of cellular phenotype: cocultivation of hepatocytes and nonparenchymal cells. FASEB J. **13,** 1883, 1999.
7. Bhatia, S.N., Yarmush, M.L., and Toner, M. Controlling cell interactions by micropatterning in co-cultures: Hepatocytes and 3T3 fibroblasts. J. Biomed. Mater. Res. **34,** 189, 1997.
8. Yamato, M., Kwon, O.H., Hirose, M., Kikuchi, A., and Okano, T. Novel patterned cell coculture utilizing thermally

responsive grafted polymer surfaces. J. Biomed. Mater. Res. **55,** 137, 2001.
9. Miltenyi, S., Muller, W., Weichel, W., and Radbruch, A. High gradient magnetic cell separation with MACS. Cytometry **11,** 231, 1990.
10. Moore, L.R., Zborowski, M., Sun, L., and Chalmers, J.J. Lymphocyte fractionation using immunomagnetic colloid and a dipole magnet flow cell sorter. J. Biochem. Biophys. Methods **37,** 11, 1998.
11. Radbruch, A., Mechtold, B., Thiel, A., Miltenyi, S., and Pfluger, E. High-gradient magnetic cell sorting. Methods Cell Biol. **42,** 387, 1994.
12. Lewin, M., Carlesso, N., Tung, C.H., Tang, X.W., Cory, D., Scadden, D.T., and Weissleder, R. Tat peptide-derivatized magnetic nanoparticles allow in vivo tracking and recovery of progenitor cells. Nat. Biotechnol. **18,** 410, 2000.
13. Shinkai, M., Yanase, M., Honda, H., Wakabayashi, T., Yoshida, J., and Kobayashi, T. Intracellular hyperthermia for cancer using magnetite cationic liposomes: In vitro study. Jpn. J. Cancer Res. **87,** 1179, 1996.
14. Nagatani, N., Shinkai, M., Honda, H., and Kobayashi, T. Development of a new transformation method using magnetite cationic liposomes and magnetic selection of transformed cells. Biotechnol. Tech. **12,** 525, 1998.
15. Yanase, M., Shinkai, M., Honda, H., Wakabayashi, T., Yoshida, J., and Kobayashi, T. Intracellular hyperthermia for cancer using magnetite cationic liposomes: An in vivo study. Jpn. J. Cancer Res. **89,** 463, 1998.
16. Ito, A., Shinkai, M., Honda, H., and Kobayashi, T. Heat-inducible TNF-α gene therapy combined with hyperthermia using magnetic nanoparticles as a novel tumor-targeted therapy. Cancer Gene Ther. **8,** 649, 2001.
17. Ito, A., Tanaka, K., Kondo, K., Shinkai, M., Honda, H., Matsumoto, K., Saida, T., and Kobayashi, T. Tumor regression by combined immunotherapy and hyperthermia using magnetic nanoparticles in an experimental subcutaneous murine melanoma. Cancer Sci. **94,** 308, 2003.
18. Seglen, P.O. Preparation of isolated rat liver cells. Methods Cell Biol. **13,** 29, 1976.
19. Yamada, K., Kamihira, M., and Iijima, S. Self-organization of liver constitutive cells mediated by artificial matrix and improvement of liver functions in long-term culture. Biochem. Eng. J. **8,** 135, 2001.
20. Owen, C.S., and Sykes, N.L. Magnetic labeling and cell sorting. J. Immunol. Methods **73,** 41, 1984.
21. Shinkai, M., Le, B., Honda, H., Yoshikawa, K., Shimizu, K., Saga, S., Wakabayashi, T., Yoshida, J., and Kobayashi, T. Targeting hyperthermia for renal cell carcinoma using human MN antigen-specific magnetoliposomes. Jpn. J. Cancer Res. **92,** 1138, 2001.
22. Hirose, M., Yamato, M., Kwon, O.H., Harimoto, M., Kushida, A., Shimizu, T., Kikuchi, A., and Okano, T. Temperature-responsive surface for novel co-culture systems of hepatocytes with endothelial cells: 2–D patterned and double layered co-cultures. Yonsei Med. J. **41,** 803, 2000.
23. Shimizu, T., Yamato, M., Kikuchi, A., and Okano, T. Cell sheet engineering for myocardial tissue reconstruction. Biomaterials **24,** 2309, 2003.
24. Shimizu, T., Yamato, M., Isoi, Y., Akutsu, T., Setomaru, T., Abe, K., Kikuchi, A., Umezu, M., and Okano, T. Fabrication of pulsatile cardiac tissue grafts using a novel 3–dimensional cell sheet manipulation technique and temperature-responsive cell culture surfaces. Circ. Res. **90,** 40, 2002.
25. Harimoto, M., Yamato, M., Hirose, M., Takahashi, C., Isoi, Y., Kikuchi, A., and Okano, T. Novel approach for achieving double-layered cell sheets co-culture: Overlaying endothelial cell sheets onto monolayer hepatocytes utilizing temperature-responsive culture dishes. J. Biomed. Mater. Res. **62,** 464, 2002.
26. Mironov, V., Boland, T., Trusk, T., Forgacs, G., and Markwald, R.R. Organ printing: computer-aided jet-based 3D tissue engineering. Trends Biotechnol. **21,** 157, 2003.
27. Kushida, A., Yamato, M., Konno, C., Kikuchi, A., Sakurai, Y., and Okano, T. Decrease in culture temperature releases monolayer endothelial cell sheets together with deposited fibronectin matrix from temperature-responsive culture surfaces. J. Biomed. Mater. Res. **45,** 355, 1999.
28. Gregory, P.G., Connolly, C.K., Gillis, B.E., and Sullivan, S.J. The effect of coculture with nonparenchymal cells on porcine hepatocyte function. Cell Transplant. **10,** 731, 2001.
29. Shimaoka, S., Nakamura, T., and Ichihara, A. Stimulation of growth of primary cultured adult rat hepatocytes without growth factors by coculture with nonparenchymal liver cells. Exp. Cell Res. **172,** 228, 1987.
30. Villafuerte, B.C., Koop, B.L., Pao. C.I., Gu, L., Birdsong, G.G., and Phillips, L.S. Coculture of primary rat hepatocytes and nonparenchymal cells permits expression of insulin-like growth factor binding protein-3 in vitro. Endocrinology **134,** 2044, 1994.
31. Bhandari, R.N., Riccalton, L.A., Lewis, A.L., Fry, J.R., Hammond, A.H., Tendler, S.J., and Shakesheff, K.M. Liver tissue engineering: A role for co-culture systems in modifying hepatocyte function and viability. Tissue Eng. **7,** 345, 2001.
32. Morin, O., Goulet, F., and Normand, G. Liver sinusoidal endothelial cells: Isolation, purification, characterization and interaction with hepatocytes. In Morin, O., Goulet, F., and Normand, G., eds. Cell Biology Reviews, Vol. 15. New York: Springer International, 1988, pp. 1–73.
33. Goulet, F., Normand, C., and Morin, O. Cellular interactions promote tissue-specific function, biomatrix deposition and junctional communication of primary cultured hepatocytes. Hepatology **8,** 1010, 1988.

Address reprint requests to:
Takeshi Kobayashi, Ph.D.
Department of Biotechnology
School of Engineering
Nagoya University
Furo-cho, Chikusa-Ku, Nagoya 464–8603, Japan

E-mail: takeshi@nubio.nagoya-u.ac.jp

ELSEVIER

Biochemical Engineering Journal 20 (2004) 119–125

Biochemical Engineering Journal

www.elsevier.com/locate/bej

A new methodology of mesenchymal stem cell expansion using magnetic nanoparticles

Akira Ito[a], Eri Hibino[a], Hiroyuki Honda[a], Ken-ichiro Hata[b], Hideaki Kagami[c], Minoru Ueda[d], Takeshi Kobayashi[a,*]

[a] *Department of Biotechnology, School of Engineering, Nagoya University, Nagoya 464-8603, Japan*
[b] *Genetic and Regenerative Medical Center, School of Medicine, Nagoya University, Nagoya 466-8550, Japan*
[c] *J-TEC Endowed Chair in Tissue Engineering, School of Medicine, Nagoya University, Nagoya 466-8550, Japan*
[d] *Department of Oral and Maxillofacial Surgery, School of Medicine, Nagoya University, Nagoya 466-8550, Japan*

Received 8 May 2003; accepted after revision 4 September 2003

Abstract

Mesenchymal stem cells (MSCs), which can differentiate into multiple mesodermal tissues, may be useful for autologous cell transplantation, if MSCs, which are isolated from bone marrow in small numbers, can be expanded in vitro. We developed a combined methodological approach to enrich and proliferate MSCs in vitro using magnetic nanoparticles. Our magnetite cationic liposomes (MCLs), which have a positive surface charge in order to improve adsorption, accumulated in MSCs at a concentration of 20 pg of magnetite per cell. The MCLs exhibited no toxicity against MSCs in proliferation and differentiation to osteoblasts and adipocytes. The MSCs magnetically labeled by MCLs were enriched using magnets and then cultured, resulting in much higher density (seeding density, 1000 cells/cm^2) than in ordinary culture (seeding density, 18 cells/cm^2). When MSCs were seeded at high density using MCLs, there was a 5-fold increase in the number of cells, compared to culture prepared without MCLs. Our results suggest that this novel culture method using magnetic nanoparticles can be used to efficiently expand MSCs for clinical application.

Keywords: Mesenchymal stem cells; Cell culture; Proliferation; Liposomes; Magnetic particles

1. Introduction

Bone marrow-derived mesenchymal stem cells (MSCs) can differentiate into osteoblasts, chondrocytes, adipocytes, muscle cells or nerve cells in vitro and in vivo [1–4]. Because MSCs can easily be obtained by bone marrow aspiration, transplantation of bone marrow MSCs may provide a new treatment for regeneration of mesenchymal tissues [3]. However, marrow aspiration of too great a volume causes damage and pain to the donor. Thus, it is difficult to obtain the large number of MSCs required for regeneration of injured tissues. Expansion of MSCs in vitro is a necessary step in clinical application of MSCs.

Despites the great interest in MSCs, there is still no well-defined protocol for isolation and expansion of MSCs in culture. Most experiments have been conducted using MSCs isolated primarily from bone marrow aspirates by their tight adherence to plastic dishes, as described by Friedenstein et al. [5]. However, this method for isolating cells does not help increase the number of MSCs, because there is only a small number of MSCs within bone marrow aspirate. Pittenger et al. reported that only a small percentage (0.0001–0.01%) of bone marrow aspirate cells that attached to the culture dishes were MSCs [1]. Also, culture volume needs to be large, since there are numerous nonadherent cells such as hematopoietic cells that must be diluted and removed by washing and changes in medium, resulting in low-density culture of MSCs. In such a low-density culture, MSCs do not proliferate immediately, and they require much time to develop into colonies. Low-density culture is not efficient for cell proliferation because growth factors including autocrine [6–9], paracrine [9], and juxtacrine [10] factors play an important role in cell growth. In the present study, we developed a new method for producing high-density culture, using magnetic nanoparticles to promote expansion of MSCs.

Magnetic particles ranging in size from nanometers to micrometers have been used in an increasing number of biological and medical applications. The unique feature of

* Corresponding author. Tel.: +81-52-789-3213; fax: +81-52-789-3214.
E-mail address: takeshi@nubio.nagoya-u.ac.jp (T. Kobayashi).

1369-703X/$ – see front matter © 2003 Published by Elsevier B.V.
doi:10.1016/j.bej.2003.09.018

magnetic particles is their reaction to magnetic force. Magnetic particles are attracted to high magnetic flux density, and this feature is used for drug targeting and bioseparation including cell sorting [11–14]. We have developed magnetite cationic liposomes (MCLs), which are cationic liposomes containing magnetic nanoparticles, in order to improve accumulation of magnetic nanoparticles in target cells using electrostatic interaction with the cell membrane [15]. MCLs have been used as carriers to introduce DNA into cells [16], and as heat generating mediators for cancer therapy [17–19]. In the present study, magnetic forces were used to move MSCs labeled with MCLs, to hold them in situ, and to culture them at high density. We investigated the applicability of this combined methodological approach to enrichment and proliferation of MSCs in vitro.

2. Materials and methods

2.1. Preparation of magnetite cationic liposomes

The magnetite (Fe_3O_4; average particle size, 10 nm) used as the core of the MCLs was kindly donated by Toda Kogyo (Hiroshima, Japan). The MCLs were prepared with colloidal magnetite and a lipid mixture consisting of *N*-(α-trimethylammonioacetyl)-didodecyl-D-glutamate chloride, dilauroylphosphatidyl-choline, and dioleoylphosphatidyl-ethanolamine in a 1:2:2 molar ratio, as described previously [15].

2.2. Effects of MCLs on proliferation and multilineage differentiation of MSCs

Human bone marrow MSCs were obtained from BioWhittaker (secondary cultures, Walkersville, MD), which are uniformly positive for SH2, SH3, CD29 and CD44 and negative for CD14, CD34 and CD45, and they can differentiate into osteoblasts, chondrocytes, adipocytes. MSCs were cultured in Mesenchymal Stem Cell Growth Medium (MSCGM, BioWhittaker) containing fetal bovine serum, L-glutamine, streptomycin sulfate and potassium penicillin G as antibiotics. Uptake of MCLs by cells was examined using a published method [15]. Briefly, MSCs (2.75×10^5 cells) were seeded into a 100 mm dish (Asahi Techno Glass, Chiba, Japan) with 10 ml of MSCGM. After 24 h of incubation, the medium was replaced by MSCGM containing MCLs (net magnetite concentration, 100 pg per cell), and the cells were incubated again. To assay magnetite uptake, cells were sampled periodically, and iron concentration and cell number were measured using the potassium thiocyanate method [20] and the dye-exclusion method with trypan blue, respectively.

Osteogenic or adipogenic conversion of MSCs was determined according to procedures reported by Pittenger et al., with some modifications [1]. For osteogenic differentiation, cells were seeded at 3.1×10^3 cells/cm^2 in a 100 mm dish and maintained for 17 days in osteogenic induction medium (BioWhittaker). Then, alkaline phosphatase activity was determined using the method of Bessey et al. [21]. For adipogenic differentiation, cells were seeded at 2.1×10^4 cells per six-well culture plate (Asahi Techno Glass) and maintained in MSCGM for 2 days. The cells were exposed to adipogenic induction medium (BioWhittaker) for 3 days, followed by 2 days of culture in adipogenic maintenance medium (BioWhittaker). After three complete cycles of induction/maintenance, the cells were cultured for 5 more days in adipogenic maintenance medium. Lipid in the cells was stained with oil-red O [22], and the percentage of the total area of the confluent culture that was stained was analyzed by image analysis software (LIA 32, by Dr. Kazukiyo Yamamoto, Nagoya University).

2.3. Expansion of MSCs using MCLs

At 4 h after addition of the MCLs, 1000 MSCs (corresponding to the MSCs in 1 ml of bone marrow aspirate) were seeded into a 100 mm dish (Asahi Techno Glass) with 10 ml of MSCGM. A cylindrical neodymium magnet (diameter, 2.2 cm; height, 1 cm; 4000 Gauss) was then placed under the 100 mm dish to provide magnetic force vertical to the dish, and the dish was shaken in a figure-eight pattern using a shaker (Taitec, Tokyo) for 10 min. The magnetic flux of the magnet was measured by a hand-held Gauss meter (F. W. Bell, Orlando, FL). As a control experiment, 1000 MSCs without MCL addition were seeded into a 100 mm dish with 10 ml of MSCGM, and the dish was shaken in a figure-eight pattern using a shaker for 10 min. At 7 days after cell seeding, the number of viable cells was determined using a WST assay kit (Dojindo, Kumamoto, Japan) according to the manufacturer's protocol. At 14 days after seeding, the cells were fixed with 10% formaldehyde solution and stained with 0.2% crystal violet solution to visualize the cells accumulated by magnetic force.

2.4. Statistical analysis

Statistical significance of differences in numbers of MSCs was evaluated using the Mann–Whitney rank sum test. Differences were considered statistically significant when the P value was less than 0.05.

3. Results

3.1. Magnetic nanoparticle uptake by MSCs and its effect on proliferation and multilineage differentiation

Uptake of magnetic nanoparticles began rapidly, and maximum uptake (20 pg per cell) was achieved 4 h after addition (Fig. 1A). Subsequently, the amount of magnetite per cell decreased due to dilution as a result of cell growth. Growth

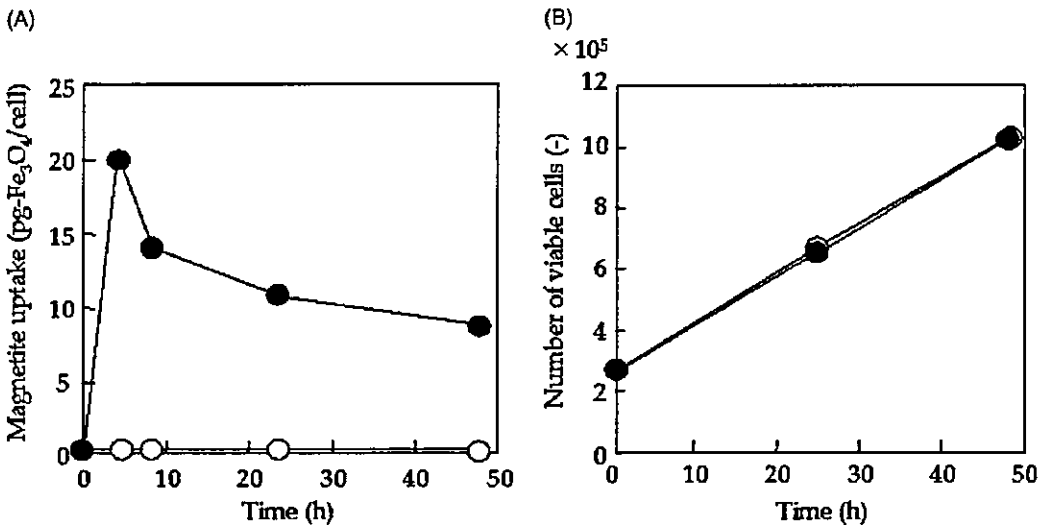

Fig. 1. Magnetite uptake and proliferation of MSCs. Magnetite uptake after addition of MCLs (100 pg per cell) was measured by the potassium thiocyanate method (A). Toxicity of MCLs against MSC cell growth was examined after addition of MCLs (B). Open circles, MCL(−)MSCs; closed circles, MCL(+)MSCs. Data points are means of triplicate.

of MSCs in medium containing MCLs (MCL(+)MSCs) was compared to growth of MSCs in medium without MCLs (MCL(−)MSCs) (Fig. 1B). MCLs did not inhibit nor stimulate growth of MSCs.

Osteogenic differentiation of MCL(+)MSCs transferred into osteogenic medium was attained 17 days after transfer. MSCs incubated in osteogenic medium changed shape from fibroblastic to polygonal, and formed calcium nodules (Fig. 2A). There was no significant difference in shape between MCL(−)MSCs in osteogenic medium (Fig. 2A-III) and MCL(+)MSCs in osteogenic medium (Fig. 2A-IV). MCL(+)MSCs and MCL(−)MSCs had similar levels of alkaline phosphatase activity after incubation in MSCGM and osteogenic induction medium (Fig. 2B).

Adipogenic induction of MCL(+)MSCs was attained after culturing in adipogenic medium, as indicated by accumulation of lipid-rich vacuoles within cells and the presence of Oil-red O-positive cells (Fig. 3). MCL(+)MSCs and MCL(−)MSCs had similar percentage areas of Oil-red O-positive cells (45 and 40%, respectively), as indicated by analysis using imaging software.

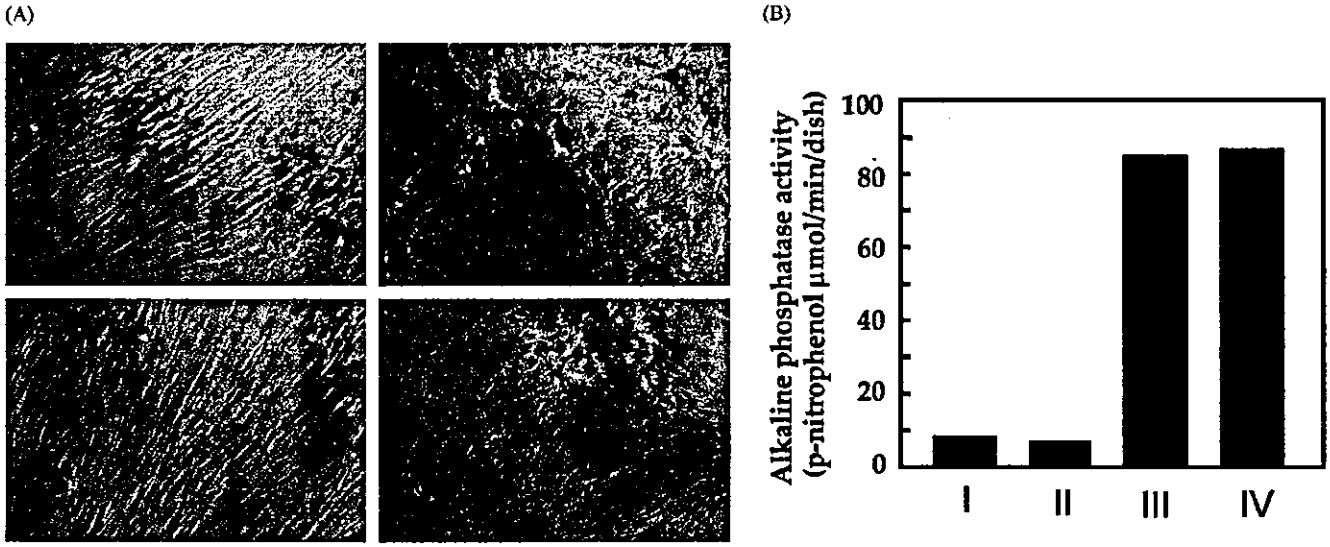

Fig. 2. Osteogenic potential of magnetically labeled MSCs. MSCs were incubated in medium containing MCLs for 4 h, and were then incubated in osteogenic induction medium for 17 days. Representative photographs (A; scale bar, 100 μm) and alkaline phosphatase activity at 28 days after medium change are shown (B; data points are means of triplicate). I, MCL(−)MSCs incubated in MSCGM; II, MCL(+)MSCs incubated in MSCGM; III, MCL(−)MSCs incubated in osteogenic induction medium; IV, MCL(+)MSCs incubated in osteogenic induction medium.

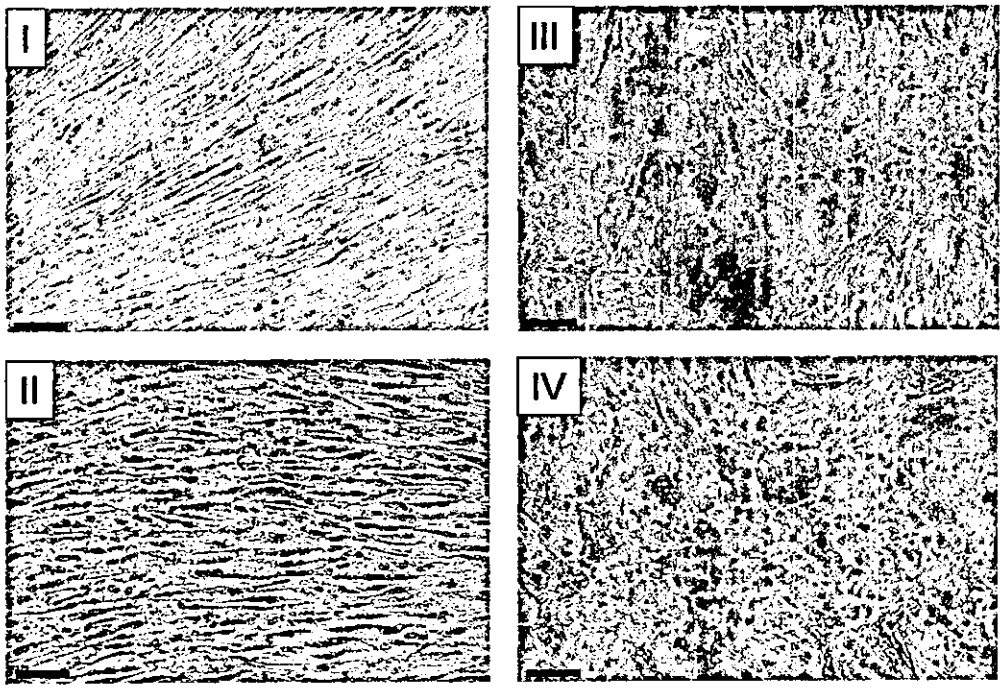

Fig. 3. Adipogenic potential of magnetically labeled MSCs. Representative photographs of Oil-red O staining are shown (scale bar, 100 μm). MSCs were incubated in medium containing MCLs for 4 h, and were then incubated in adipogenic induction/maintenance medium for 20 days. I, MCL(−)MSCs incubated in adipogenic maintenance medium; II, MCL(+)MSCs incubated in adipogenic maintenance medium; III, MCL(−)MSCs incubated in adipogenic induction/maintenance medium; IV, MCL(+)MSCs incubated in adipogenic induction/maintenance medium.

3.2. Expansion of MSCs using magnetic nanoparticles and magnetic force

Fig. 4 shows the magnetic flux density at the surface of the magnet. The magnetic density was highest at the edge of the magnet. To investigate the state of cells trapped by the magnetic force, the cells were stained with crystal violet at 14 days after cell seeding (Fig. 5). MCL(−)MSCs formed scattered colonies throughout the dish. In contrast, MCL(+)MSCs accumulated circumferentially along the edge of the magnet at the center of dish where the magnet was positioned. Since magnetic particles are attracted to high magnetic flux density, MCL(+)MSCs were attracted where the magnet was positioned. Moreover, it was assumed that the pattern of accumulation was due to the magnetic flux created by the magnet, since the magnetic density was highest at the periphery of the magnet (Fig. 4). MCL(+)MSCs and MCL(−)MSCs were cultured for 14 days so that the visible colonies of MCL(−)MSCs could be fully developed. However, daily microscopic observation revealed that the MCL(+)MSCs grew to over-confluence during this long-term culture. Therefore, the growth area regulated by the magnetic force was the value obtained for confluent MCL(+)MSCs culture; this value was approximately 1 cm^2, as indicated by image analysis. These results suggest that the MCL(+)MSCs were seeded at 1000 cells/cm^2, which was a much higher concentration than that of MCL(−)MSCs (18 cells/cm^2; 1000 cells per 55 cm^2 dish).

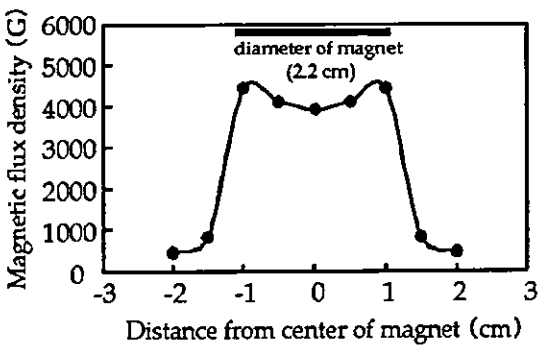

Fig. 4. Magnetic flux density around a neodymium magnet. The magnetic flux of the magnet was measured by a hand-held Gauss meter.

MCL(+)MSCs attached to the dish at higher cell density than MCL(−)MSCs at 1 day after seeding, and then proliferated progressively as shown in Fig. 6A. The MCL(+)MSCs achieved confluence on Day 7, at which time the number of viable cells was counted. A total of 2.2×10^4 cells were counted, corresponding to the number of cells in 1 cm^2 of confluent culture (approximately 2×10^4 cells/cm^2). This was five-fold greater than the number obtained for MCL(−)MSCs (Fig. 6B); the difference was significant ($P < 0.05$).

4. Discussion

Methods for expansion of MSCs are in great demand for clinical applications. One approach to expansion of MSCs

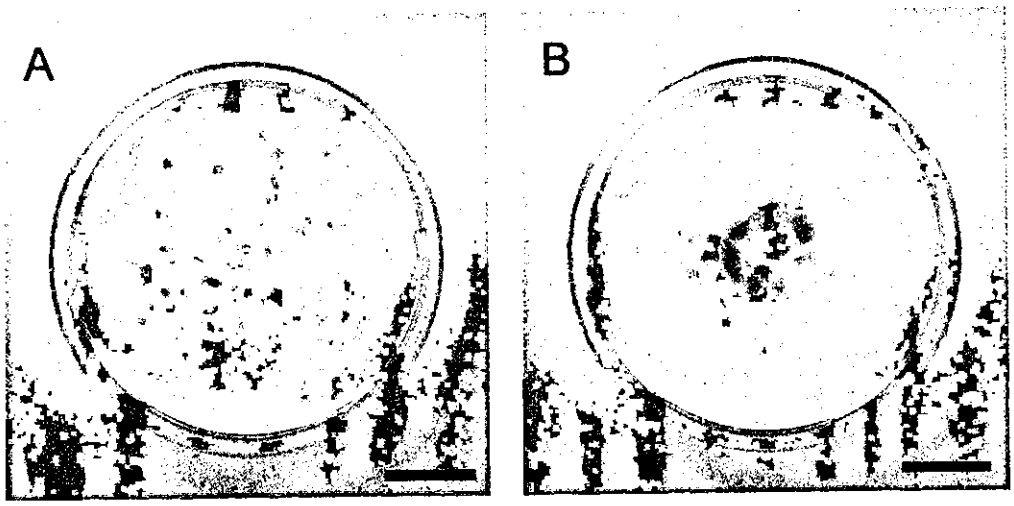

Fig. 5. State of MSCs accumulated by magnetic force. Representative photographs of crystal violet staining at 14 days after cell seeding (scale bar, 2 cm). (A) MCL(−)MSCs; (B) MCL(+)MSCs.

is identification of growth factors involved in self-renewal of MSCs. Tsutsumi et al. reported that fibroblast growth factor-2 (FGF-2) increased the growth rate of rabbit, canine and human bone marrow MSCs [23]. However, the mechanism by which FGF-2 maintains proliferation without differentiation is unknown. In general, clinical applications of cytokines should be pursued with caution because of the unknown functions of cytokines. Alternatively, growth factors such as cytokines are produced by cells themselves and act as autocrine factors. Huss et al. reported that autocrine factors such as stem cell factor (SCF) and interleukin-6 (IL-6) were involved in proliferation and differentiation of a canine bone marrow-derived cell line, and that an increase in local cell concentration was associated with cell viability [24]. In our preliminary experiments using canine bone marrow cells (1 ml of canine bone marrow including approximately 1000 MSCs in 4 ml medium), the number of cells increased more rapidly under the condition of the same MSCs concentration when the cells were cultured in a 35 mm dish than when they were cultured in a 100 mm dish. These results prompted us to use magnetic force, since MSCs can be separated by using magnets even when the culture volume increases. In the present study, we demonstrated the efficacy of "high-density culture" using magnetic nanoparticles and magnetic force. When MSCs were seeded at high density using MCLs, the number of cells obtained was five-fold greater than the number obtained from culture without MCLs (Fig. 6). These results suggest that growth factors including autocrine, paracrine, and juxtacrine factors are involved in proliferation of MSCs. "High-density culture" using magnetic nanoparticles provides a new methodology for expansion of MSCs.

Toxicity of magnetic nanoparticles is an important issue for clinical applications. We previously used MCLs as

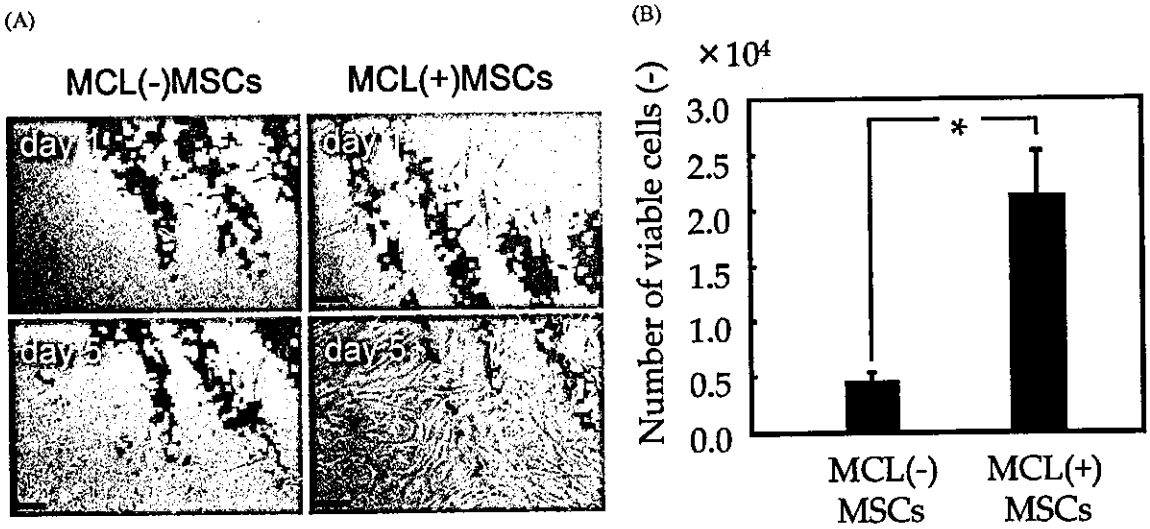

Fig. 6. Expansion of MSCs using magnetic nanoparticles. Representative photograph of MCL(−) (A, left) and MCL(+) (A, right) MSCs at 1 and 5 days after cell seeding (scale bar, 100 μm), and numbers of viable cells at 7 days after cell seeding (B, $n = 3$, $^*P < 0.05$), are shown.

heat-generating material for hyperthermia, and examined their toxicity against cancer cells [15]. No toxicity against cell proliferation was observed when the magnetite concentration was <100 pg per cell. In the present study, we observed no toxicity against MSC proliferation (Fig. 1B) or differentiation (Figs. 2 and 3) when the magnetite concentration was 100 pg per cell. At an MCL concentration of 100 pg per cell, 20% of the magnetic nanoparticles were incorporated into MSCs (Fig. 1A), and these magnetically labeled MSCs were attracted by magnetic force, suggesting that magnetite uptake of 20 pg per cell is sufficient for accumulation of cells using magnets (Fig. 5). In the present study, we did not investigate effects of cell accumulation by various types of magnets. There is a need for investigation of the effects of various types of magnets, including differences in size, shape and magnetic flux density.

The use of antibodies against MSCs is a promising approach to isolation of MSCs from bone marrow aspirates. We previously developed antibody-immobilized magnetoliposomes (AMLs) for cancer therapy [25–28]. Combined use of antibody against MSCs immobilized on magnetic nanoparticles and culture of MSCs using magnetic nanoparticles provide an effective method for isolating and expanding MSCs. Recently, many researchers have used various antibodies to isolate or characterize MSCs [29–31]. However, further investigation is needed to determine the most appropriate antibodies for these purposes.

In conclusion, we propose a novel methodology using magnetic nanoparticles to expand very small numbers of MSCs. This novel methodology, which involves use of high-density culture, can be applied to tissue engineering for expansion of MSCs that are isolated in small numbers.

Acknowledgements

The authors would like to thank Toda Kogyo Co. for supplying the magnetite. This work was supported in part by the 21st Century COE Program "Nature-Guided Materials Processing" of the Ministry of Education, Sports, Science and Technology.

References

[1] M.F. Pittenger, A.M. Mackay, S.C. Beck, R.K. Jaiswal, R. Douglas, J.D. Mosca, M.A. Moorman, D.W. Simonetti, S. Craig, D.R. Marshak, Multilineage potential of adult human mesenchymal stem cells, Science 284 (1999) 143–147.

[2] S. Makino, K. Fukuda, S. Miyoshi, F. Konishi, H. Kodama, J. Pan, M. Sano, T. Takahashi, S. Hori, H. Abe, J. Hata, A. Umezawa, S. Ogawa, Cardiomyocytes can be generated from marrow stromal cells in vitro, J. Clin. Invest. 103 (1999) 697–705.

[3] R.J. Deans, A.B. Moseley, Mesenchymal stem cells: biology and potential clinical uses, Exp. Hematol. 28 (2000) 875–884.

[4] G.C. Kopen, D.J. Prockop, D.G. Phinney, Marrow stromal cells migrate throughout forebrain and cerebellum, and they differentiate into astrocytes after injection into neonatal mouse brains, Proc. Natl. Acad. Sci. U.S.A. 96 (1999) 10711–10716.

[5] A.J. Friedenstein, J.F. Gorskaja, N.N. Kulagina, Fibroblast precursors in normal and irradiated mouse hematopoietic organs, Exp. Hematol. 4 (1976) 267–274.

[6] Y.S. Maruyama, Y.S. Tohda, K. Nagata, T. Suzuki, I. Murohashi, N. Nara, Role of humoral and cellular factors on the growth of blast progenitors of acute myeloblastic leukemia in serum-free culture, Hematol. Pathol. 4 (1990) 115–123.

[7] I.A. Reilly, R. Kozlowski, N.H. Russell, The role of cell contact and autostimulatory soluble factors in the proliferation of blast cells in acute myeloblastic leukemia, Leukemia 3 (1989) 145–150.

[8] H. Gloeckner, H.D. Lemke, New miniaturized hollow-fiber bioreactor for in vivo like cell culture, cell expansion, and production of cell-derived products, Biotechnol. Prog. 17 (2001) 828–831.

[9] A. Kimura, O. Katoh, H. Hyodo, S. Kusumi, A. Kuramoto, Autocrine and/or paracrine mechanism operate during the growth of human bone marrow fibroblasts, Br. J. Haematol. 78 (1991) 469–473.

[10] U.K. Ehmann, M.K. Terris, Juxtacrine stimulation of normal and malignant human bladder epithelial cell proliferation, J. Urol. 167 (2002) 735–741.

[11] S. Miltenyi, W. Muller, W. Weichel, A. Radbruch, High gradient magnetic cell separation with MACS, Cytometry 11 (1990) 231–238.

[12] L.R. Moore, M. Zborowski, L. Sun, J.J. Chalmers, Lymphocyte fractionation using immunomagnetic colloid and a dipole magnet flow cell sorter, J. Biochem. Biophys. Meth. 37 (1998) 11–33.

[13] A. Radbruch, B. Mechtold, A. Thiel, S. Miltenyi, E. Pfluger, High-gradient magnetic cell sorting, Meth. Cell Biol. 42 (1994) 387–403.

[14] M. Lewin, N. Carlesso, C.H. Tung, X.W. Tang, D. Cory, D.T. Scadden, R. Weissleder, Tat peptide-derivatized magnetic nanoparticles allow in vivo tracking and recovery of progenitor cells, Nat. Biotechnol. 18 (2000) 410–414.

[15] M. Shinkai, M. Yanase, H. Honda, T. Wakabayashi, J. Yoshida, T. Kobayashi, Intracellular hyperthermia for cancer using magnetite cationic liposomes: in vitro study, Jpn. J. Cancer Res. 87 (1996) 1179–1183.

[16] N. Nagatani, M. Shinkai, H. Honda, T. Kobayashi, Development of a new transformation method using magnetite cationic liposomes and magnetic selection of transformed cells, Biotechnol. Tech. 12 (1998) 525–528.

[17] M. Yanase, M. Shinkai, H. Honda, T. Wakabayashi, J. Yoshida, T. Kobayashi, Intracellular hyperthermia for cancer using magnetite cationic liposomes: an in vivo study, Jpn. J. Cancer Res. 89 (1998) 463–469.

[18] A. Ito, M. Shinkai, H. Honda, T. Kobayashi, Heat-inducible TNF-alpha gene therapy combined with hyperthermia using magnetic nanoparticles as a novel tumor-targeted therapy, Cancer Gene Ther. 8 (2001) 649–654.

[19] A. Ito, K. Tanaka, K. Kondo, M. Shinkai, H. Honda, K. Matsumoto, T. Saida, T. Kobayashi, Tumor regression by combined immunotherapy and hyperthermia using magnetic nanoparticles in an experimental subcutaneous murine melanoma, Cancer Sci. 94 (2003) 308–313.

[20] C.S. Owen, N.L. Sykes, Magnetic labeling and cell sorting, J. Immunol. Meth. 73 (1984) 41–48.

[21] O.A. Bessey, O.H. Lowly, M.J. Brock, A method for the rapid determination of alkaline phosphatase with five cubic millimeters of serum, J. Biol. Chem. 164 (1946) 321–329.

[22] G.J. Hausman, Techniques for studying adipocytes, Stain Technol. 56 (1981) 149–154.

[23] S. Tsutsumi, A. Shimazu, K. Miyazaki, H. Pan, C. Koike, E. Yoshida, K. Takagishi, Y. Kato, Retention of multilineage differentiation potential of mesenchymal cells during proliferation in response to FGF, Biochem. Biophys. Res. Commun. 288 (2001) 413–419.

[24] R. Huss, C.A. Hoy, H.J. Deeg, Contact- and growth factor-dependent survival in a canine marrow-derived stromal cell line, Blood 85 (1995) 2414–2421.

[25] M. Shinkai, M. Suzuki, S. Iijima, T. Kobayashi, Antibody-conjugated magnetoliposomes for targeting cancer cells and their application in hyperthermia, Biotechnol. Appl. Biochem. 21 (1995) 125–137.

[26] M. Suzuki, M. Shinkai, M. Kamihira, T. Kobayashi, Preparation and characteristics of magnetite-labelled antibody with the use of poly(ethylene glycol) derivatives, Biotechnol. Appl. Biochem. 21 (1995) 335–345.
[27] B. Le, M. Shinkai, T. Kitade, H. Honda, J. Yoshida, T. Wakabayashi, T. Kobayashi, Preparation of tumor-specific magnetoliposomes and their application for hyperthermia, J. Chem. Eng. Jpn. 34 (2001) 66–72.
[28] M. Shinkai, B. Le, H. Honda, K. Yoshikawa, K. Shimizu, S. Saga, T. Wakabayashi, J. Yoshida, T. Kobayashi, Targeting hyperthermia for renal cell carcinoma using human MN antigen-specific magnetoliposomes, Jpn. J. Cancer Res. 92 (2001) 1138–1145.
[29] S.E. Haynesworth, M.A. Baber, A.I. Caplan, Cell surface antigens on human marrow-derived mesenchymal cells are detected by monoclonal antibodies, Bone 13 (1992) 69–80.
[30] F.P. Barry, R.E. Boynton, S. Haynesworth, J.M. Murphy, J. Zaia, The monoclonal antibody SH-2, raised against human mesenchymal stem cells, recognizes an epitope on endoglin (CD105), Biochem. Biophys. Res. Commun. 265 (1999) 134–139.
[31] N. Quirici, D. Soligo, P. Bossolasco, F. Servida, C. Lumini, G.L. Deliliers, Isolation of bone marrow mesenchymal stem cells by anti-nerve growth factor receptor antibodies, Exp. Hematol. 30 (2002) 783–791.

High-Resolution Submicron Patterning of Self-Assembled Monolayers Using a Molecular Fluorine Laser at 157 nm

Florin Andrei Nae,*,† Nagahiro Saito,‡ Atsushi Hozumi,§ and Osamu Takai†

EcoTopia Science Institute, Nagoya University, Chikusa, Nagoya 464-8603, Japan, Department of Molecular Design and Engineering, Graduate School of Engineering, Nagoya University, Chikusa, Nagoya 464-8603, Japan, and National Institute of Advanced Industrial Science and Technology (AIST), 2266-98, Anagahora, Shimo-shidami, Moriyama-ku, Nagoya 463-8560, Japan

Received July 28, 2004. In Final Form: October 22, 2004

Using a molecular fluorine laser at 157 nm wavelength, submicron patterning of organosilane self-assembled monolayers (SAMs) is demonstrated utilizing mask-contact photolithography. An organosilane, namely, octadecyltrimethoxysilane [ODS, $CH_3(CH_2)_{17}Si(OCH_3)_3$], SAM is chemisorbed onto Si substrates covered with a 2 nm thick oxide layer and subsequently patterned using the laser. The optical path of the laser beam and the photomask−sample space are evacuated and then backfilled and purged with nitrogen during laser firing. The resulting pattern is investigated using various measurement techniques. The scanning probe microscopy images show that patterns are transferred to the SAM-covered Si substrates and that 500 nm features are successfully photoprinted in this way.

Introduction

Producing increasingly smaller features in materials by laser irradiation requires increasingly shorter wavelength sources. The molecular fluorine (F_2) laser at 157 nm produces the shortest wavelength photons available from any commercial laser.[1,2] This short wavelength coupled with the high 7.9 eV photon energy has decreased the smallest feature sizes which can be produced by laser processing and also widened the range of materials that can be patterned with submicron resolution.[3] Furthermore, shorter wavelengths are diffracted less, thus allowing smaller feature sizes to be produced. On the other hand, self-assembled monolayers (SAMs) are a class of materials increasingly considered for technological applications requiring patterning due to their simplicity of use and environmental friendliness.[4,5] Sub-100-nm high lateral resolution patterning and lithography of SAMs can be achieved by soft lithography, as in the case of nanoimprint lithography, by scanning probe microscopy (SPM) that includes dip-pen or anodic oxidation nanolithography, or by energetic beams, as in the case of X-ray or electron beam lithography.[6−11] However, photolithography, being an established and mature technique and able to transfer an entire pattern on a relatively large surface at one time, is still expected to play a major role in the future.

Organosilane SAMs, formed on hydroxyl-terminated surfaces through silane coupling chemistry, have attracted much attention as promising candidates for ultrathin photoresist films.[12−14] Conventional polymer resists can be modified or structured with energetic beams using photons, electrons, or ions. However, the efficiency of the polymer resists is limited by their relatively high thicknesses and intermolecular distances. Because of their nanometer size thickness and small intermolecular distance of less than 1 nm, the potential resolution of SAMs is higher than that for polymer resists. Nanometer-thick SAMs of organosilanes on silicon surfaces can assist in advancing conventional photolithography by serving as sacrificial resists, i.e., by chemically modifying the SAM so that chemically different regions vary in their susceptibility to attack by wet etches.[15,16] SAM patterning using an F_2 laser is therefore considered to be of a practical interest since photolithography is still the most used patterning method in the electronics industry and there is persistent demand for smaller features to be patterned. Also, from a fundamental research point of view, the results presented hereafter can be useful since this is, to our present knowledge,[17] one of the first reports on

* To whom correspondence should be addressed. E-mail: nae@plasma.numse.nagoya-u.ac.jp. Tel: +81-52-789-2796. Fax: +81-52-736-3260.

† EcoTopia Science Institute, Nagoya University.

‡ Department of Molecular Design and Engineering, Nagoya University.

§ National Institute of Advanced Industrial Science and Technology (AIST).

(1) Rice, J. K.; Hays, A. K.; Woodworth, J. R. *Appl. Phys. Lett.* **1977**, *31*, 31.

(2) Pummer, H.; Hohla, K.; Diegelmann, M.; Reilly, J. P. *Opt. Commun.* **1979**, *28*, 104.

(3) Rothschild, M.; Bloomstein, T. M.; Fedynyshyn, T. H.; Liberman, V.; Mowers, W.; Sinta, R.; Switkes, M.; Grenville, A.; Orvek, K. *J. Fluorine Chem.* **2003**, *122*, 3−10.

(4) Sagiv, J. *J. Am. Chem. Soc.* **1980**, *102*, 92.

(5) Takahara, A.; Sakata, H.; Morita, M.; Koga, T.; Otsuka, H. *Compos. Interfaces* **2003**, *10*, 489−504.

(6) Lercel, M. J.; Whelan, C. S.; Craighead, H. G.; Seshadri, K.; Allara, D. L. *J. Vac. Sci. Technol. B* **1996**, *14*, 4085−4090.

(7) Odom, T. W.; Thalladi, V. R.; Love, J. C.; Whitesides, G. M. *J. Am. Chem. Soc.* **2002**, *124*, 12112−12113.

(8) Snow, E. S.; Campbell, P. M.; Perkins, F. K. *Proc. IEEE* **1997**, *85*, 601−611.

(9) Austin, M. D.; Chou, S. Y. *Nano Lett.* **2003**, *3*, 1687−1690.

(10) Ginger, D. S.; Zhang, H.; Mirkin, C. A. *Angew. Chem., Int. Ed.* **2003**, *43*, 30−45.

(11) Wang, X. J.; Hu, W. C.; Ramasubramaniam, R.; Bernstein, G. H.; Snider, G.; Lieberman, M. *Langmuir* **2003**, *19*, 9748−9758.

(12) Ulman, A. *An Introduction to Ultrathin Organic Films*; Academic Press: Boston, MA, 1991.

(13) Dulcey, C. S.; George, J. H., Jr.; Krauthamer, V.; Stenger, D. A.; Fare, T. L.; Calvert, J. M. *Science* **1992**, *252*, 551.

(14) Sugimura, H.; Hanji, T.; Taka, O.; Masuda, T.; Misawa, H. *Electrochim. Acta* **2001**, *47*, 103−107.

(15) Dressick, W. J.; Calvert, J. M. *Jpn. J. Appl. Phys.* **1993**, *32*, 5829.

(16) Calvert, J. M. *J. Vac. Sci. Technol. B* **1993**, *11*, 2155.

(17) Smith, R. K.; Lewis, P. A.; Weiss, P. S. *Prog. Surf. Sci.* **2004**, *75*, 1−68.

10.1021/la0480944 CCC: $30.25
Published on Web 01/20/2005

photodegradation of octadecyltrimethoxysilane (ODS) SAMs using light at 157 nm.

In this study, we performed preliminary research whose main aim was to evaluate the potential spatial resolution of an F_2 laser exposure system for submicron patterning of an organosilane SAM. Another aim was to provide insight into the photochemistry mechanism involved. Previous research,[14] concerned with SAM patterning using vacuum ultraviolet light at 172 nm generated by an excimer Xe_2* lamp, has shown that, under specific experimental conditions, the photochemistry of alkylsilanes at 172 nm may not be a simple conversion of the hydrophobic alkyl headgroups into hydrophilic oxidized products such as, for e.g., −COOH and −CHO. Therefore, it is of interest to compare the photoirradiation results at 157 nm with those at other wavelengths.

X-ray photoelectron spectroscopy (XPS), ellipsometry, and contact angle measurements were performed to characterize the effect of the laser irradiation on the SAM. Atomic and lateral force microscopy (AFM and LFM, respectively) were employed to image the patterns, revealing that 500 nm features were successfully patterned.

Experimental Section

SAM Preparation. Sample substrates cut from Si(100) 125 mm diameter wafers (n-type, resistivity = 8−12 Ω cm, ShinEtsu Handoutai) were first sonicated for 10 min in ethanol, acetone, and toluene, in this order, and then photochemically cleaned by a vacuum ultraviolet/ozone method.[18,19] Consequently, a thin oxide layer of about 2 nm in thickness, whose surface was most likely terminated with OH groups, formed on the Si substrates. The oxide surface became almost completely hydrophilic, with the water contact angles found to be less than 5°. Static water contact angles of the sample surfaces were measured at ambient temperature and humidity in air using an automated contact angle goniometer (CRUSS DSA 10-Mk2) based on the sessile drop method. All the contact angles were determined by averaging values measured at five different points on each sample surface, and the error was estimated to be 2%.

An alkylsilane SAM was then formed on the Si substrates by a chemical vapor deposition (CVD) method using octadecyltrimethoxysilane [Tokyo Kasei Organic Chemicals, $CH_3(CH_2)_{17}Si(OCH_3)_3$] as a precursor, which has a vapor pressure of 2 Torr at 150 °C. Details of this method were described elsewhere.[19] The ODS SAM's thickness was estimated using an ellipsometer (PZ2000, Philips) with a He−Ne laser (λ = 632.8 nm), a 45° polarizer, and the angle of incidence set at 70° from the surface normal. The optical constants N_{Si} = 3.875 and K_{Si} = −0.023, where N is the index of refraction, and K is the absorption coefficient, respectively, were used for the silicon substrate, and values of N_{ov} = 1.460 and K_{ov} = 0 were used for the overlayer, assumed to be transparent at this wavelength and considered to consist of both the SAM and the chemical oxide on the Si substrate. The overlayer thicknesses were typically within ±0.2 nm on each sample and had a standard deviation of ±0.1 nm for a given spot on a sample.

Ellipsometry data were collected at 10 spots per sample, with three or more measurements performed at each individual location, with measurement error estimated to be less than 0.1 nm. Since obtained values constituted the sum of the SAM's thickness and the oxide, actual monolayer thickness could be determined by subtracting oxide thickness from the total. Using this method, the SAM thickness was estimated to be approximately 1.68−1.7 nm. After SAM formation, the water contact angle was checked for a few selected samples with the average value found to be 106.3°.

(18) Sugimura, H.; Nakagiri, N. *J. Photopolym. Sci. Technol.* **1997**, *10*, 661.
(19) Hozumi, A.; Ushiyama, K.; Sugimura, H.; Takai, O. *Langmuir* **1999**, *15*, 7600.

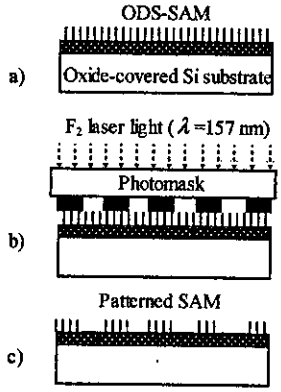

Figure 1. Schematic illustration of the F_2 laser patterning procedure of an ODS SAM: (a) chemisorption of the ODS SAM on an oxide-covered Si surface; (b) laser irradiation through a photomask in contact with the ODS SAM; (c) the patterned ODS SAM.

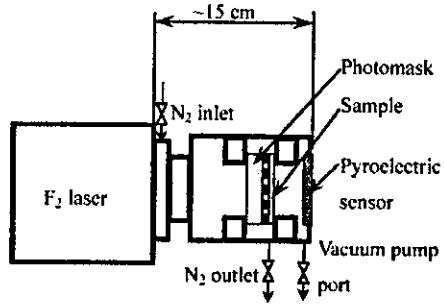

Figure 2. Schematic illustration of the F_2 laser lithography system.

F_2 Laser System Preparation. As schematically illustrated in Figure 1, the ODS SAM prepared on the Si substrate was patterned through mask-contact photolithography. The experimental setup is schematically shown in Figure 2. The ODS SAM sample was placed in a chamber, subsequently evacuated at a scroll dry rotary pump (Phil Sato OFS-M-150Z) ultimate pressure of 13 Pa. One of the main issues associated with 157 nm radiation is the high absorption of photons by molecular oxygen, water, and organic molecules.[3] To counter this effect, the beam path can be either evacuated or purged with an inert gas such as nitrogen. We chose to purge the beam path with 99.999% purity nitrogen gas at 10 L/min during experiments. The photomask used was a traditionally binary one and consisted of a 6.3 mm thick fused quartz glass plate covered with a 100 nm thick metallic absorber (chromium-based) pattern having features ranging from 500 nm to 5 μm. A pulsed F_2 laser (TUI Laser ExciStar S-200), at a radiation wavelength of 157 nm and set up at a repetition rate of 200 Hz, was used as a light source. Pulse duration at full width at half-maximum was 15 ns. The active laser medium inside the laser tube was a gas mixture of helium and a small fraction (less than 0.2 vol %) of F_2 gas. The pressure in the laser tube, right after changing the premix gas, was around 5800 hPa. The size of the laser beam at the aperture was 3 mm × 3 mm. The laser-delivered energy was checked near the ODS SAM location using a pyroelectric sensor (Ophir Optronics PE50). The average indicated energy was found to vary significantly according to the static and dynamic lifetime of the laser-tube premix gas and environmental noise, for instance, the noise generated by the laser electrostatic dust remover and blower motor. Without photomask and immediately after changing the premix gas, the measured energy approached the laser specified value of 1 mJ/pulse, as seen from a typical energy histogram in Figure 3. Regarding the energy transmitted through the photomask, since fused quartz is nearly opaque at 157 nm,[20] typical measured values were small, in the range of 15−20 μJ/pulse. Therefore,

(20) Hideo, H.; Yoshiaki, I. *Nucl. Instrum. Methods Phys. Res., Sect. B* **2000**, *166−167*, 691−697.

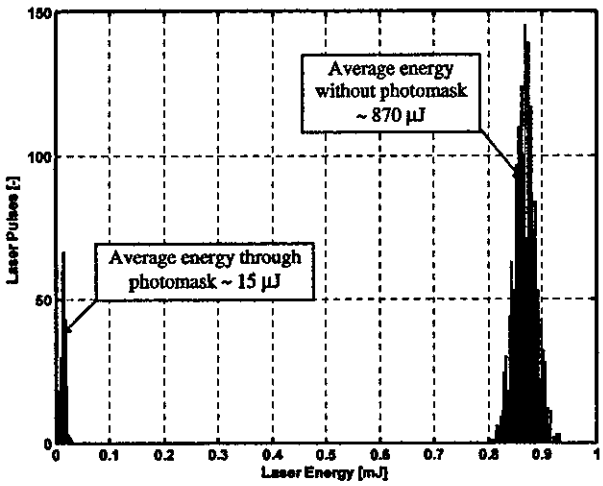

Figure 3. Measured laser energy, with and without photomask.

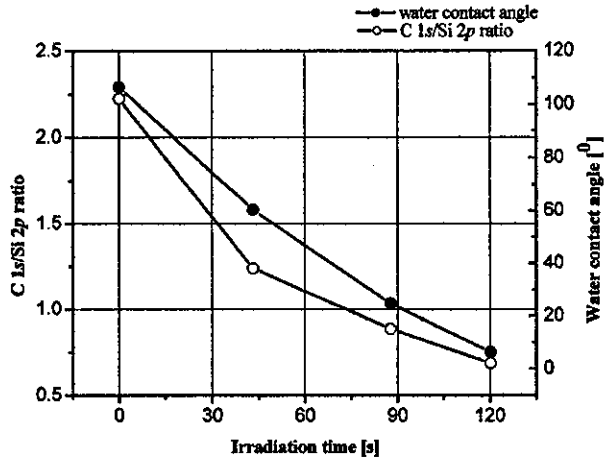

Figure 4. Effect of irradiation time on the ODS SAM. Evolution of the water contact angle, represented by the solid line with closed circles, and the C/Si intensity ratio, shown as a solid line with open circles.

the fluence at the ODS SAM surface was roughly estimated as 160–200 μJ/cm^2/pulse. Based on this value and trial-and-error experiments, we have found that the ODS SAM is sufficiently irradiated after a 30 min exposure. The best patterns were obtained after performing an initial photocleaning of the photomask; namely, the photomask was irradiated for 20 min prior to experiments without a sample attached to it.

SPM and XPS Measurements. SPM is an excellent analytical tool for imaging different regions of patterned SAMs or other nanostructured surfaces. The sensitivity of silicon tips to different structures on the surface is very high, even without chemical modification of the tips.[21] The morphology of patterned sample surfaces was imaged using a scanning probe microscope (Seiko Instruments SPA-300HV +SPI-3800N) with an all-Si cantilever (Park Scientific Ultralever ULCT20), having a spring constant of 1.9 N/m, a resonance frequency of 53 kHz, and a nominal radius of less than 10 nm, as given by the manufacturer. Images were obtained while operating the instrument in contact mode in ambient conditions. The scan rate of the probe ranged from 0.1 to 0.25 Hz, and images were recorded with a 512 × 512 pixel resolution. AFM and LFM images were acquired simultaneously, using the fast scanning direction perpendicular to the major cantilever axis. Results are presented as raw, unfiltered data. A scan head with a maximum range of 150 μm × 150 μm was used. XPS measurements were performed using an instrument (Shimadzu Kratos AXIS, 1.0 × 10^{-7} Torr) with the X-ray line at Mg Kα (1253.6 eV), operated at 12 kV and 10 mA. XP narrow scan spectra of C 1s and Si 2p photoemission lines were acquired, with an analyzer pass energy of 20 eV. All peak positions analyzed by XPS were normalized to that of the Si 2p peak appearing at 99.3 eV, which was referenced to an n-type Si wafer.

Results and Discussion

The procedure described in the Experimental Section resulted in reproducible fabrication of patterned ODS SAM surfaces with features having different shapes and sizes ranging from 500 nm to 5 μm. All samples were irradiated for 30 min with the F_2 laser. During irradiation, since many organic compounds are very absorptive at 157 nm,[3] F_2 laser light dissociatively excites the chemical bonds, e.g., C–C and C–H, and forms radicals.[22] Also, even when purging with nitrogen after evacuating the air, we expect some molecular oxygen to exist along the beam path and in the test chamber, for instance, due to the residual pressure of more than 10 Pa after the evacuation or because some air remains trapped between photomask and sample. Dissociation of residual H_2O content in the enclosure or in the nonperfect nitrogen gas can also be a source of oxygen. Light between 133 and 200 nm is absorbed by organic molecules and oxygen molecules, and simultaneously, oxygen atoms both in several excited states (i.e., O[^{1}D] or O[^{1}S]) as well as in the ground state (O[^{3}P]) are generated.[23] Since the activated oxygen has a strong oxidative reactivity to organic molecules, the degraded ODS SAM further reacts with activated oxygen and is converted in an environmental friendly manner to volatile species such as H_2O and CO_2 and to a small amount of volatile organic compounds.[24,25] The ODS SAM is finally removed from the irradiated regions. Since silicon does not readily form volatile compounds under these conditions, a residual film of SiO_x containing a small amount of carbon remains at the surface of the substrates. Activated oxygen is too short-lived to diffuse appreciable distances and thus must be generated in situ within a region of unconverted SAM in order to continue the conversion process. This is one reason we decided to purge the chamber with nitrogen during irradiation, since in this way the nitrogen flow may act as a carrier for the water or oxygen present in the nonperfect nitrogen gas as well as for the photodecomposition byproducts. Carrying molecular oxygen and water near the substrate can generate atomic oxygen near the location of the unconverted SAM. Despite the beneficial effects of oxygen, the primary constraint with it is its strong absorption at 157 nm of approximately 1%/m/ppm.[26] Considering that the optical beam path in commercial microsteppers is several meters long, to ensure enough laser fluence at the work piece, this restricts the practical levels of oxygen in commercial applications to the range of 10–1000 ppm. This concern was the main reason in keeping the sample as near as possible to the laser aperture, as indicated in Figure 2.

Changes in water contact angles of the directly photoirradiated ODS SAMs are plotted in Figure 4. As photoirradiation was prolonged, water contact angles decreased. The contact angles became less than 5° after

(21) Bar, G.; Rubin, S.; Martin, T.; Taylor, T. N.; Swanson, B. I.; Zawodzinski, T. A.; Chow, J. T.; Ferraris, J. P. *Supramol. Sci.* **1997**, *4*, 11–19.

(22) Holländer, A.; Klemberg-Sapieha, J. E.; Wertheimer, M. R. *Macromolecules* **1994**, *27*, 2893.

(23) Amimoto, S. T.; Force, A. P.; Gulotty, R. G., Jr.; Wiesenfeld, J. R. *J. Chem. Phys.* **1979**, *71*, 3640.

(24) Vig, J. R. In *Treatise on Clean Surface Technology*; Mittal, K. L., Ed.; Kluwer Academic/Plenum: New York, 1987.

(25) Okabe, H. *Photochemistry of Small Molecules*; John Wiley & Sons: New York, 1978.

(26) Bates, A. K.; Rothschild, M.; Bloomstein, T. M.; Fedynyshyn, T. H.; Kunz, R. R.; Liberman, V.; Switkes, M. *IBM J. Res. Dev.* **2001**, *45*, 605–614.

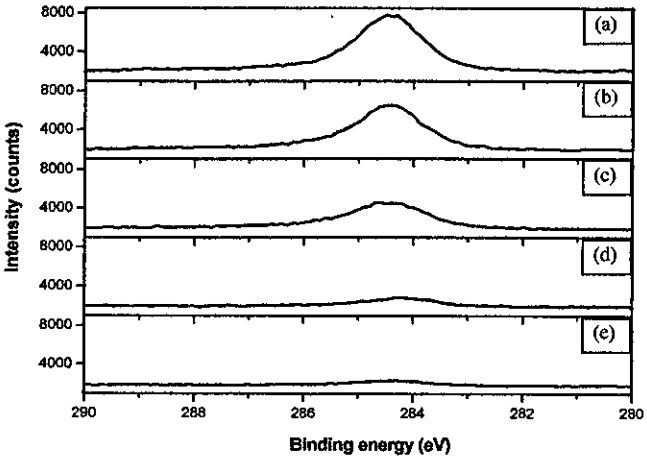

Figure 5. XPS C 1s peaks: (a) unirradiated ODS SAM, (b) after 45 s of irradiation, (c) after 90 s of irradiation, (d) after 120 s of irradiation, and (e) the clean SiO_2/Si substrate.

irradiation for 120 s, indicating that photoirradiated surfaces became completely hydrophilic.

XPS Results. We also confirmed based on XPS measurements that the carbon intensity level on the photoirradiated SAM surfaces decreased with photoirradiation time. Figure 4 presents the carbon/silicon (C/Si) intensity ratio as a function of irradiation time. The ratio decreases with irradiation time. The decrease in the C/Si ratio can be attributed to a reduction in the amount of carbon within the converted surface film.

Figure 5 shows C 1s XPS narrow scans of the unirradiated and irradiated ODS SAMs as well as a spectrum of a photochemically cleaned Si surface. The peak in the C 1s spectrum of the undegraded ODS SAM was assigned to emissions from alkyl chains. After laser irradiation, the peak intensity of the alkyl chains has decreased since ODS molecules were removed gradually. The intensity after 120 s of irradiation (spectrum d) becomes almost equal to that of a clean Si surface, prior to SAM deposition, i.e., a background level (spectrum e). The origin of C 1s signals from the cleaned Si surface is carbon contamination adsorbed prior to the XPS measurement. Such contamination most likely had to be adsorbed on the irradiated SAM surface as well. Oxidized products, such as −COOH and −CHO groups, do not appear at 287−289 eV in the C 1s XPS spectra.[27] Although further detailed research is needed, lithography at 157 nm looks promising for patterning a large variety of SAMs, since it may depend on photoinduced cleavage of C−C bonds and subsequent decomposition of organic molecules.[14] Figure 6 shows the narrow scan of the Si 2p region. The solid lines with open squares show the unirradiated ODS SAM, the solid lines with circles show the irradiated ODS SAM after 120 s of irradiation time, and the continuous curve shows the photocleaned substrate. With increasing irradiation time, the intensities of both the Si peak at 99.3 eV and the Si−O peak at 103.3 eV increase, approaching the values for the clean substrate.

SPM Results. Figure 7 shows a 10 μm × 10 μm LFM image consisting of lines and spaces having a width of 500 nm each. Such a clear pattern was observed on larger surfaces too (not shown here), up to the maximum range of 150 μm × 150 μm of the SPM scan head and within the total patterned area of around 3 mm × 3 mm dictated by the aperture of the laser. A larger value for the friction

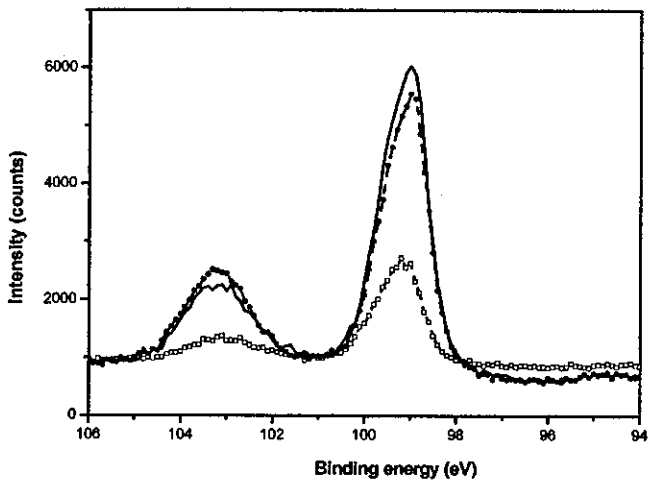

Figure 6. XPS Si 2p region. The solid lines with open squares show the unirradiated ODS SAM, the solid lines with circles show the irradiated ODS SAM after 120 s of irradiation time, and the continuous curve shows the photocleaned substrate.

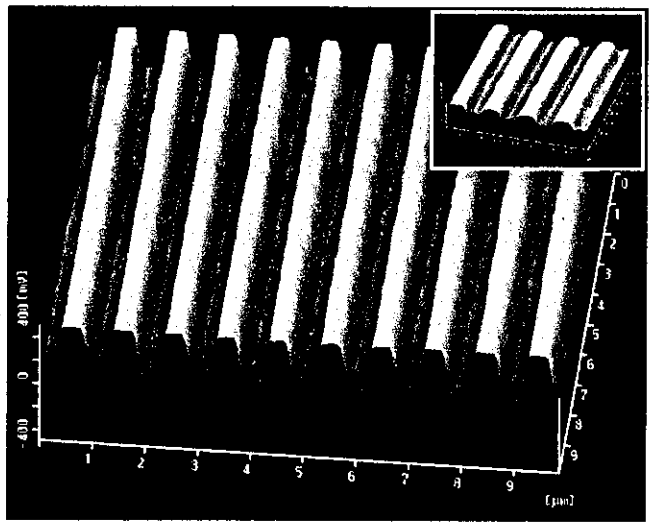

Figure 7. Lateral force microscopy image of the line-space patterned region.

force is representative for photodegraded areas.[28] These areas, which exhibited stronger lateral force than the hydrophobic, undegraded SAM surfaces, had to be hydrophilic as shown in Figure 4. Hydrophilic regions of photodegraded SAMs chemically interact with the AFM-probe surface, which due to its surface oxide is also hydrophilic, leading to higher friction values. In such a case, hydrogen bondings may form between the sample and probe surfaces.

An inevitable shortcoming of photolithography is that its patterning resolution is degraded by penumbral blurring effects together with diffraction and reflection of light. The inset in Figure 7 shows, for clarity, a 4 μm × 4 μm area. At the top of the unirradiated regions, an additional thin line is visible. We believe this line to be caused by laser light diffraction at the edge of the chromium pattern on the photomask. Despite this undesirable effect, the width of this line is estimated to be around 100 nm, providing an indication that the photolithographic process can create 100 nm features, or even less, on ODS SAMs.

Topographies of the patterned SAMs were also acquired in order to provide more insight into the process that took

(27) Beamson, G.; Briggs, D. *High-Resolution XPS of Organic Polymers*; John Wiley & Sons: Chichester, 1992.

(28) Sugimura, H.; Nakagiri, N. *Appl. Phys. A* **1998**, *66*, S427.